ORIGINAL PAPER

Multi-response optimization of MIL-101 synthesis for selectively adsorbing N-compounds from fuels

Mohamad Songolzadeh[1] · Mansooreh Soleimani[1] · Maryam Takht Ravanchi[2]

Abstract

In this work, MIL-101, a metal organic framework, has been synthesized and examined in the adsorptive denitrogenation process. Due to the importance of adsorption capacity and selectivity, the effects of synthesis parameters including metal type, reagent ratio, time and temperature on the MIL-101 performance were investigated by measuring quinoline (QUI) separation from iso-octane. The optimum conditions were determined using a Taguchi experimental design and the multi-response optimization (multivariate statistical) method. Based on the arithmetic mean of normalized QUI adsorption capacity and QUI/dibenzothiophene (DBT) selectivity, as the objective function, the optimum value of synthesis parameters were found to be manganese as metal type in the structure, 180 °C for synthesis temperature, 15 h for synthesis time and 1.00 for reagent molar ratio. Under these conditions, QUI adsorption capacity and QUI/DBT selectivity were 19.3 mg-N/g-Ads. and 24.6, respectively. Accordingly, the arithmetic mean between normalized values of these measured parameters was equal to 1.10, which is in good agreement with the predicted value. The MIL-101 produced under optimum conditions was characterized by determining its specific surface area, X-ray powder diffraction patterns and Fourier transform infrared spectroscopy. Finally, isotherm and kinetic studies indicate that the Langmuir isotherm and pseudo-first-order model can successfully describe the experimental data.

Keywords MIL-101 · Adsorptive denitrogenation · Taguchi experimental design · Multi-response optimization

1 Introduction

Metal–organic frameworks (MOFs) are one of the fastest growing materials that have attracted much attention. MOFs are tunable crystalline hybrid networks with high porosity, specific functionality and selective interaction (Li et al. 2010a, b). In the last decade, these materials have interested researchers as their properties such as pore size and shape, surface area and special physicochemical surface properties can easily be regulated and modified by altering the connectivity of organic–inorganic moieties (Hu et al. 2018). MOFs can be used with different roles in a large number of processes including gas adsorption and storage, adsorptive removal of hazardous materials, catalysis, drug delivery, carriers for nanomaterials, electrode materials, luminescence and magnetism (Li et al. 2010a, b).

Due to the problems of the presence of nitrogen-containing compounds (NCCs) in fuel such as NO_x emission and spoiling hydrodesulfurization (HDS) process, the separation of NCCs before removing sulfur-containing compounds (SCCs) is crucial (Khan et al. 2017). Adsorptive denitrogenation (ADN) is one of the crucial technologies that are highly environmentally friendly and do not need any hydrogen usage for removing NCCs from fuel. Adsorption of NCCs from fuel is a promising process in which MOFs can be successfully utilized (Sentorun-Shalaby et al. 2013). Several MOFs have been used for ADN, among which MIL-101 had notable adsorption capacity and selectivity, for removing NCCs from fossil fuels

---

✉ Mansooreh Soleimani
Soleimanim@aut.ac.ir

Mohamad Songolzadeh
Songol89122048@gmail.com

Maryam Takht Ravanchi
maryamravanchi@gmail.com

[1] Department of Chemical Engineering, Amirkabir University of Technology, Tehran, Iran

[2] Petrochemical Research and Technology Company, National Petrochemical Company, Tehran, Iran

(Ahmed et al. 2013a). Different techniques such as changing metal ions (Songolzadeh et al. 2019) and adding Lewis acid sites (Ahmed et al. 2013a; Ahmed and Jhung 2014) have been tested to improve ADN characteristics including adsorption capacity and selectivity. Varying and optimizing reaction conditions of MOF synthesis, so far not investigated for ADN, are other effective techniques that can be used to prepare superior adsorbents for this process. Several methods such as solvothermal, slow evaporation, microwave-assisted, sonochemical, mechanochemical and electrochemical synthesis are used for the synthesis of MOFs (Ahmed and Jhung 2016). Solvothermal, a simple and environmentally friendly method, has usually been applied for the MOF synthesis. Based on numerous studies (Taheri et al. 2018; Li et al. 2011; Stock and Biswas 2011), temperature and time of synthesis, reagent concentrations and ratios, solvent and metal are fundamental effective parameters in MOF synthesis. Consequently, an alteration in any of these synthetic factors can change the adsorbent properties and separation characteristics of MOFs.

The objective of the present work is to investigate the effects of synthetic factors on the capacity of MIL-101 in the ADN process and to optimize parameters for maximum adsorption efficiency by experimental design. In this study, two compositional factors, namely the type of metal ion and the reagent ratio, and two process parameters including time and temperature were considered as extremely crucial in order to produce a high-quality MIL-101 for the ADN process. Regarding the long time needed for and the difficulty of MOF synthesis, the Taguchi method was used to design experiments, decrease the number of experiments, minimize their error, evaluate the effects of variables and optimize the performance of this process. ADN performance was determined with adsorption capacity and selectivity of quinoline which is the most common basic N-compound in liquid fuel. Therefore, a combination of two responses consisting of adsorption capacity and selectivity was applied for statistical analysis.

2 Materials and methods

2.1 Materials

Iso-octane (C_8H_{18}, 99.5%), terephthalic acid (TPA, 98.0%), N,N-dimethylformamide (DMF, 99.5%) and QUI (97.0%) were procured from Merck Company. Manganese (III) oxide (Mn_2O_3, 99.9%), vanadium pentoxide (V_2O_5, 99.0%) and chromium trioxide (CrO_3) were provided by Sigma-Aldrich Company. In this study, all chemicals were used without further purification.

Table 1 Synthetic factors and their levels for synthesizing MIL-101 (Cr), MIL-101 (V) and MIL-101 (Mn)

No. of variables	Variables	Levels		
		Level 1	Level 2	Level 3
1	Temperature, °C	120	150	180
2	Time, h	10	15	20
3	Reagent molar ratio (molar ratio of metal oxide per TPA)	0.33	0.67	1.00

2.2 MOFs synthesis

In this study, the solvothermal method was applied for the synthesis of MOFs (MIL-101). Chromium, vanadium and manganese are used in the formation of MOFs to investigate the influence of metal type on the performance of the ADN process. Other synthetic factors and their levels are presented in Table 1. To synthesize three different MIL-101s, the appropriate amounts of TPA and metal oxide with a specific molar ratio were dissolved in 25 mL DMF. The obtained material was mixed well with a magnetic stirrer for 1 h at room temperature. The mixtures were then transferred to a 25-mL Teflon-lined autoclave and heated in a programmable muffle furnace for varied times at different temperatures, as listed in Table 1. After this step, to remove the remaining unreacted TPA, the resulting powder was filtered and washed by stirring with 25 mL DMF for 8 h. The remaining solvent (DMF and water) was removed by washing twice with 25 mL deionized water and washing once with 25 mL acetone. Finally, to remove all evaporating solvents from the synthesized MOFs, they were put in a vacuum oven for 48 h at 160 °C and 21.3 kPa. The MIL-101 (Cr), MIL-101 (V) and MIL-101 (Mn) were obtained as powders with colors of light sea green, yellow-green and light brown, respectively.

2.3 Characterization

The X-ray diffraction (XRD) pattern was determined with a Philips PW 1730 diffractometer. NOVA series 1000-Quantachrome instruments were used to measure N_2 sorption isotherms at −196 °C and calculate the specific surface area of the optimum synthesized MOFs. Before BET analysis, the samples were degassed down to 10^{-4} mbar at 150 °C for 5 h. FTIR patterns of optimum samples were recorded using a Nicolet Nexus 670 spectrometer FTIR at 4 cm^{-1} resolution within the range of 4000–400 cm^{-1}.

2.4 Design of experiments

Experimental design is an efficient method to study the parameter effects and optimize various variables for obtaining the best results by fewer experiments. The Taguchi method is a well-known and fast technique that can be used for experimental design and response optimization (Montgomery 2017; Moattari et al. 2015). In this work, the effects of all the important parameters including type of metal ions, reagent ratio, time and temperature of synthesis were studied and optimized by the Taguchi method. Since the type of metal ion is qualitative, discrete and a very effective variable in MOFs synthesis, the effect of this parameter was independently investigated and was not considered as a variable in experimental design with the Taguchi approach. Based on these contents and the Taguchi approach, three orthogonal arrays with three columns and nine rows (L9) were sufficient for these experiments. The variables and results of these experiments are presented in Table 2. To eliminate unwanted errors, all the experiments were repeated three times at the same conditions and average results have been considered in the studies. The QUI adsorption capacity, QUI/DBT selectivity and the arithmetic mean of them were used as responses for optimizing variables of MOF synthesis. In this work, the arithmetic mean of these two responses, such as the Derringer function (DF) that is the most important in multi-response optimization, was proposed and investigated to optimize MIL-101 synthesis for improving ADN characteristics.

In order to describe and use this combination of responses, each response should be normalized by Eq. 1 (Antony 2000; Guria et al. 2014):

$$R_{i,j}^N = \frac{R_{i,j} - R_{i,\min}}{R_{i,\max} - R_{i,\min}} \tag{1}$$

where $R_{i,j}^N$ represents the normalized amount of the ith response at jth experimental run, $R_{i,j}$ shows the quantity of the ith response at the jth experimental run and $R_{i,\min}$ and $R_{i,\max}$ indicate minimum and maximum values of the ith response, respectively. According to the mean arithmetic, the objective function was defined by Eq. 2 (Safarzadeh and Motahhari 2014; Heidari and Razmi 2012).

$$Z_j^1 = \frac{\sum_{i=1}^{n} R_{i,j}^N}{n} \tag{2}$$

where n is the number of responses and Z_j^1 indicates the mean arithmetic.

2.5 Adsorption experiments

Stock solutions of both QUI and DBT were prepared by individually dissolving 10,000 ppm of each one in iso-octane. The solution of 200 ppm QUI and mixture of 200 ppm QUI + 200 ppm DBT were used to measure adsorption capacity and calculate QUI/DBT selectivity, respectively. Prior to the adsorption tests, the moisture of adsorbents was removed by placing them in a vacuum oven at 160 °C for 48 h. For each experiment, appropriate amounts of adsorbent (5 mg) and 5 mL of the solutions were transferred to sealed glasses and shaken at 20 °C for 24 h. Due to the long time for each adsorption test, a new rotary shaker was designed and manufactured to adequately mix a large number of specimens simultaneously. The schematic of the experimental apparatus is illustrated in Fig. 1. The rotating blade of this rotary shaker has four fins around a shaft, in which 15 sealed glasses can be placed in each fin as sliding from their head. The speed of blade rotation and temperature of the water bath tank were controlled by two controller systems. After adsorption experiments, the concentrations of QUI and DBT in the residual solution were analyzed by gas chromatograph (Agilent 7890) equipped with a flame ionization detector and HP-5 column.

The adsorption capacity of each adsorbate and QUI/DBT selectivity were calculated by Eqs. 3 and 4, respectively (Wu et al. 2014; Ahmed and Jhung 2014).

$$q_t = \frac{(C_i - C_f)V}{m} \tag{3}$$

where q_t is the amount of adsorbed component in time t, mg g^{-1}; C_i and C_f are initial and final concentrations of the adsorbate, ppm; V is the volume of the solution, mL; and m is the weight of the adsorbent, mg.

$$S = \frac{q_{QUI}/q_{DBT}}{C_{e,QUI}/C_{e,DBT}} \tag{4}$$

where S is the QUI/DBT selectivity; q_{QUI} and q_{DBT} are adsorption capacities of the adsorbents, mg g^{-1}; and $C_{e,QUI}$ and $C_{e,DBT}$ are equilibrium concentrations (ppm) of QUI and DBT in the liquid phase, respectively.

3 Results and discussion

3.1 Analysis of variance results

The influence of each parameter was analyzed by using the analysis of variance (ANOVA) statistical method. The ANOVA was based on degree of freedom (DOF), sum of

Table 2 Selected experimental array (L9) and obtained results for adsorption capacity and selectivity

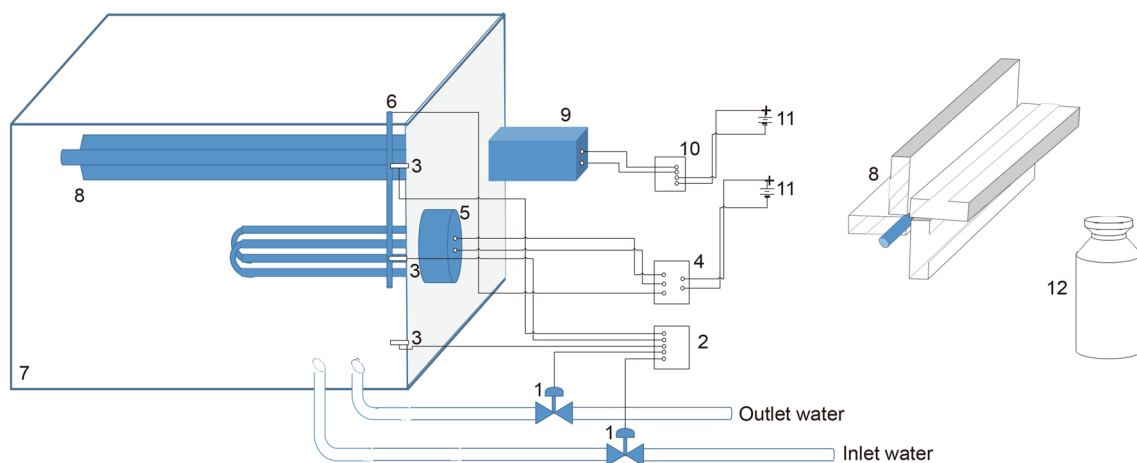| Test no.	Parameters					Observed responses			Predicted responses		
	Metal type	Tempera-ture, °C	Time, h	Reagent molar ratio		Adsorption capac-ity, mg-N/g-Ads.	Selectivity	Arithmetic mean of normal-ized capacity and selectivity	Adsorption capac-ity, mg-N/g-Ads.	Selectivity	Arithmetic mean of normal-ized capacity and selectivity
1	Cr	120	10	0.33		11.03	10.23	0.0295	11.41	9.64	0.0233
2		120	15	0.67		12.61	11.66	0.1764	13.90	13.10	0.3085
3		120	20	1.00		11.28	11.14	0.0834	13.25	11.71	0.2124
4		150	10	0.67		12.04	15.02	0.2966	12.39	12.86	0.2188
5		150	15	1.00		14.67	13.91	0.3853	15.25	14.23	0.4303
6		150	20	0.33		12.90	11.10	0.1668	13.31	12.48	0.2498
7		180	10	1.00		18.35	13.66	0.5677	16.65	15.21	0.5477
8		180	15	0.33		20.54	17.40	0.8499	18.21	16.23	0.6749
9		180	20	0.67		18.14	18.27	0.7626	17.19	16.93	0.6525
10	V	120	10	0.33		12.31	13.60	0.2476	11.77	10.90	0.0986
11		120	15	0.67		14.52	12.18	0.3003	14.26	14.36	0.3838
12		120	20	1.00		13.66	14.27	0.3483	13.61	12.97	0.2778
13		150	10	0.67		11.72	14.14	0.2407	12.75	14.12	0.2941
14		150	15	1.00		16.21	16.69	0.5903	15.61	15.49	0.5056
15		150	20	0.33		13.64	13.73	0.3231	13.67	13.74	0.3252
16		180	10	1.00		17.20	14.06	0.5247	17.01	16.47	0.6230
17		180	15	0.33		18.71	18.86	0.8189	18.57	17.49	0.7502
18		180	20	0.67		16.84	16.22	0.6025	17.55	18.19	0.7279
19	Mn	120	10	0.33		13.95	9.57	0.1538	13.98	12.95	0.3061
20		120	15	0.67		17.64	17.67	0.7093	16.47	16.41	0.5914
21		120	20	1.00		17.47	16.74	0.6589	15.83	15.01	0.4953
22		150	10	0.67		16.06	16.46	0.5722	14.96	16.17	0.5016
23		150	15	1.00		17.95	16.56	0.6763	17.83	16.54	0.7132
24		150	20	0.33		16.46	14.82	0.5200	15.88	15.79	0.5327
25		180	10	1.00		17.49	20.12	0.8110	19.22	18.52	0.8306
26		180	15	0.33		18.02	19.46	0.8092	20.78	19.54	0.9578
27		180	20	0.67		19.66	20.76	0.9535	19.76	20.23	0.9354

Fig. 1 Schematic of experimental setup (rotary shaker) for thorough mixing of samples at temperature. *Note* 1—control valves; 2—level controller; 3—level sensors; 4—temperature controller; 5—heating element; 6—temperature sensor; 7—water bath tank; 8—rotating blade; 9—electric motor; 10—variable remote control; 11—DC and AC source; 12—sealed glass for samples

Table 3 Analysis of variance (ANOVA) for QUI adsorption capacity on MIL-101, QUI/DBT selectivity and arithmetic means

Parameters	DOF	Sum of squares	Mean square	*F* value	*p* value	Contribution percentage
Capacity						
Metal type	2	34.881	17.440	9.18	0.002	21
Temperature	2	103.712	51.856	27.28	0.000	63
Time	2	23.861	11.931	6.28	0.009	14
Reagent molar ratio	2	2.719	1.359	0.72	0.502	2
Error	18	7.718	1.901	–	–	–
Total	26	44.979	–	–	–	–
Selectivity						
Metal type	2	50.160	25.078	7.22	0.005	28
Temperature	2	99.080	49.541	14.25	0.000	56
Time	2	17.220	8.611	2.48	0.112	10
Reagent molar ratio	2	10.470	5.237	1.51	0.248	6
Error	18	62.560	3.476	–	–	
Total	26	239.500	–	–	–	176.93
Z^I *(arithmetic mean of normalized capacity and selectivity)*						
Metal type	2	0.386	0.193	13.46	0.000	25
Temperature	2	0.950	0.475	33.09	0.000	61
Time	2	0.195	0.097	6.78	0.006	12
Reagent molar ratio	2	0.037	0.018	1.31	0.295	2
Error	18	0.258	0.014	–	–	–
Total	26	1.827	–	–	–	–

squares (SS), *F* value, *p* value and contribution percentage, and these factors were used to evaluate the accuracy of the model and determine the significance of each parameter (Montgomery 2017; Rahimi et al. 2015b; Loloie et al. 2017). The ANOVA results for experiments are given in detail in Table 3. QUI adsorption capacity, QUI/DBT selectivity and their arithmetic mean were studied by the ANOVA method, and the results showed that the model for capacity was comprehensively significant.

R^2 and adjusted R^2 of the QUI adsorption capacity model were obtained to be 82.8% and 75.2%, respectively. On the other hand, *F* value and *p* values, which are listed

in Table 3, were used to determine the significance of each parameter. In general, the more significant parameter has a smaller p value and larger F value in ANOVA (Rahimi et al. 2015a). Based on Table 3, temperature with a p value of ≤ 0.001 and F value of 27.3 was the most significant parameter in the capacity model. Since p values ≥ 0.050 indicated the model terms that were not significant, it is concluded that changing the reagent molar ratio, with p values equal to 0.502, did not significantly affect the QUI adsorption capacity.

In case of QUI/DBT selectivity, the obtained R^2 and R^2_{adj} were 73.9% and 62.3%, respectively. According to Table 3, the rank order of the F value of each parameter follows: (1) temperature (14.25), (2) metal type (7.22), (3) time (2.48) and (4) reagent molar ratio (1.51). Therefore, it is clear that the temperature and metal type are the two most significant factors in the QUI/DBT selectivity. Furthermore, the importance of each parameter on the response can be evaluated by calculating and comparing their percentage contribution. Based on the ANOVA results, the two most influential factors in QUI/DBT adsorption selectivity were the temperature (56%) and metal type (28%). These parameters have the greatest effect on the QUI/DBT selectivity over MIL-101.

Comparing ANOVA results for four models shows that the described model on the arithmetic mean of responses with the biggest F value (54.64), R^2 (85.86%) and adjusted R^2 (79.57%) is the best and most impressive for this optimization. Similar to other models, temperature with F value of 33.09 and metal type with F value of 13.46 are the two most significant factors, which are significantly affected QUI adsorption capacity and QUI/DBT selectivity.

3.2 Effect of adsorption characteristic parameters

3.2.1 Effect of parameters on adsorption capacity

Obtained and predicted responses for all runs, which were estimated by using the described model on the adsorption capacity, QUI/DBT selectivity and their arithmetic mean, are presented in Table 2. In the first step, the effects of each parameter on the response are investigated by comparing the average value of QUI adsorption capacity at a specific level. According to Fig. 2a, it is clear that the metal type has a great influence on the QUI adsorption capacity, so that it can be increased from 14.62 and 14.98 (mg-N/g-Ads) to 17.19 (mg-N/g-Ads) by using manganese instead of vanadium and chromium in the MIL-101 structure. Since π-complexation (between metal ions of MOFs and π-orbital of NCCs) and Lewis acid–base interaction are two predicted mechanisms for NCCs adsorption on MOFs (Wu et al. 2014; Ahmed and Jhung 2016), it can be concluded that manganese in the MIL-101 skeleton has more acidic properties and positive charge than vanadium and chromium in this skeleton (Zhang et al. 2016).

Figure 2b shows the effect of temperature on the QUI adsorption over MIL-101. Comparing Fig. 2b with a, c
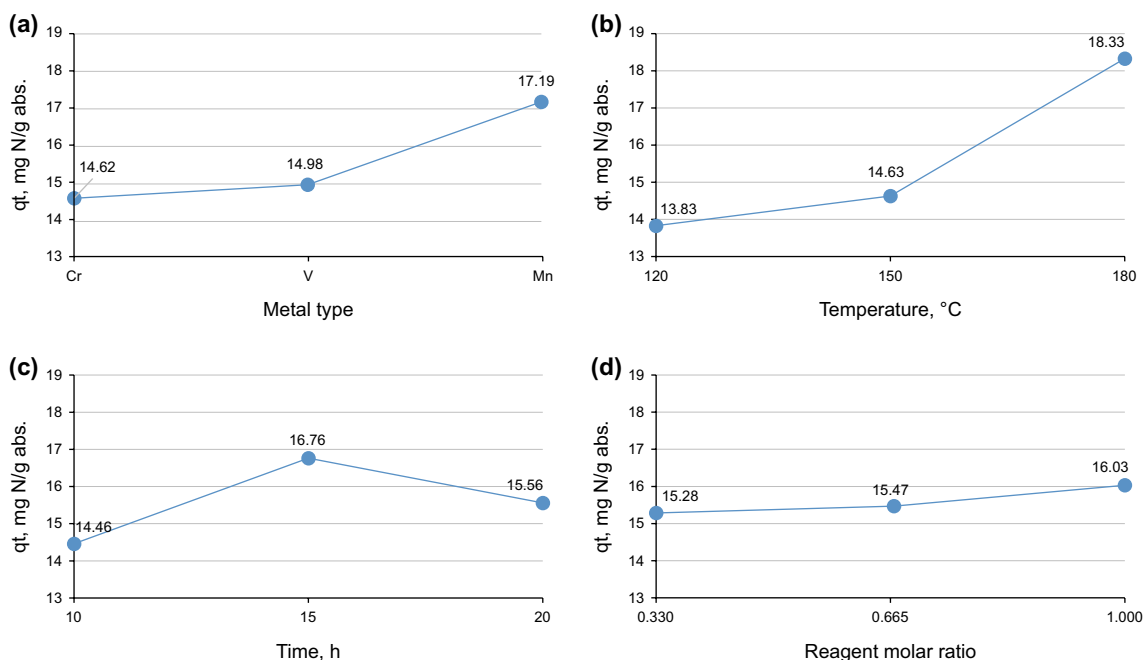

Fig. 2 Effect of parameters on QUI adsorption capacity, a metal type, b temperature, c time and d reagent molar ratio. q_t is the amount of adsorbed component at time t, mg g^{-1}
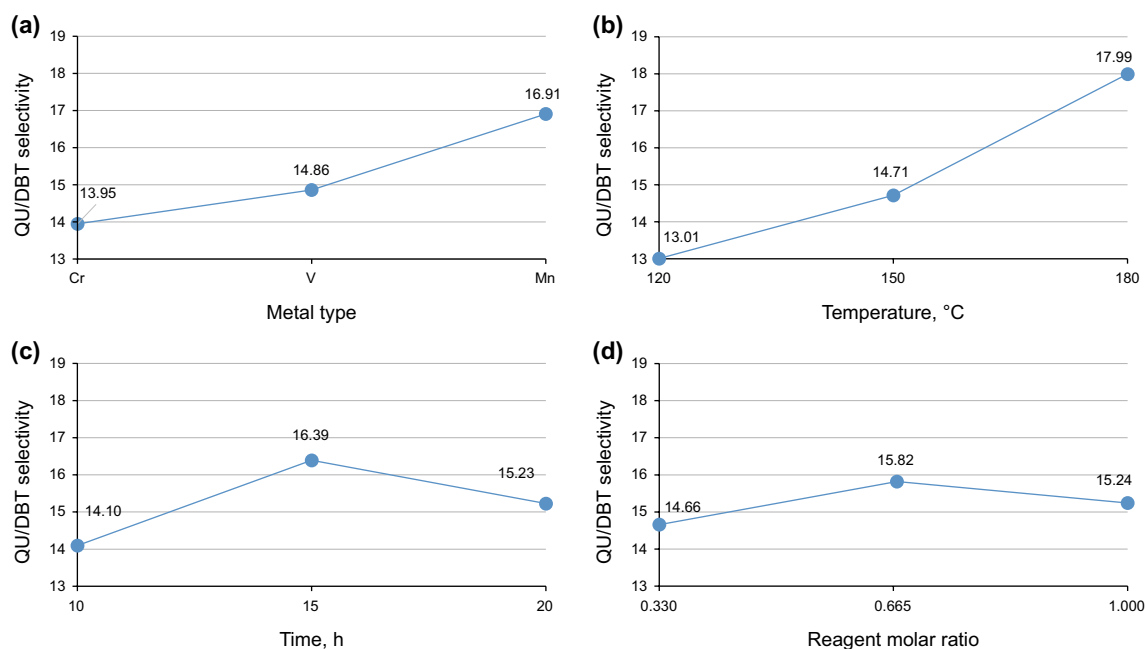
Fig. 3 Effect of parameters on QUI/DBT adsorption selectivity, **a** metal type, **b** temperature, **c** time and **d** reagent molar ratio

and d, it can be confirmed that temperature is a major and the most effective parameter on this response and QUI adsorption capacity increased dramatically (21%) when temperature was raised from 120 to 180 °C. This effect has been attributed to the fact that at higher temperatures a high solubility of reactants and large crystals of high quality would be obtained (Bag et al. 2015; Seetharaj et al. 2016; Zhang et al. 2013); therefore, synthesized MOFs in these conditions have better adsorption performance.

Figure 2c implies that the synthesis time was the parameter able to change the performance of the synthesized adsorbent. It was observed that increasing the synthesis time from 10 to 15 h leads to increasing QUI adsorption capacity from 14.46 to 16.76 mg-N/g-Ads. It is also evident that with an increase in the synthesis time, the probability of crystallization would be higher, which accelerates the QUI adsorption. However, with prolonging crystallization time, the behavior of QUI adsorption varied significantly, and it decreased sharply by increasing this time from 15 to 20 h (Aghaei and Haghighi 2015; Wee et al. 2012). This effect has been attributed to the relative large particle size that leads to long diffusion lengths and the hindrance of metal of these MOFs.

The effect of reagent molar ratio on QUI adsorption capacity is shown in Fig. 2d. According to mechanisms of NCCs adsorption on MOFs, the QUI adsorption capacity did not significantly depend on the molar ratio of the reactants, because this parameter affected the topological

pattern of MOFs and did not affect the metal cluster geometric structure.

3.2.2 Effect of parameters on QUI/DBT selectivity

The effect of each synthesis parameter on the QUI/DBT selectivity over MIL-101 is illustrated in Fig. 3. According to the predicted mechanisms for NCC adsorption on MOFs (Wu et al. 2014; Ahmed and Jhung 2016), the acidic properties and positive charge of these adsorbents play an important role in adsorption selectivity. Changing the metal type would affect both acidic properties and positive charge of synthesized MOFs; thus, varying metal type in MOFs skeleton can modify ADN characteristics including adsorption capacity and selectivity. As mentioned earlier, the metal type in the MIL-101 structure was selected between Cr (level 1), V (level 2) and Mn (level 3). The correlation of selectivity with metal type is roughly similar to the correlation of adsorption capacity with it. Figure 3a indicates that the QUI/DBT selectivity increased from 14.0 and 14.9 to 16.9, by using manganese oxide instead of vanadium and chromium oxide in the MIL-101 synthesis process.

It was observed that increasing temperature from 120 to 180 °C leads to raising QUI/DBT selectivity from 13.0 to 18.0 (Fig. 3b). It is also evident that with an increase in temperature, larger crystals with high quality are formed (Bag et al. 2015; Zhang et al. 2013; Seetharaj et al. 2016), which enhance the probability of selective QUI adsorption on the active sites of the adsorbent (metals in MOFs structure).

Figure 3c shows the effect of the synthesis time on the QUI/DBT selectivity over synthesized MOFs. It was considered that the maximum selectivity of QUI/DBT separation was related to the medium crystallization time (15 h). In case of increasing synthesis time from level 1 (10 h) to level 2 (15 h), the selectivity was increased by providing the crystals enough time to grow well-formed and consequently letting QUI and DBT to easily come in contact with metal sites of MOFs which can selectively adsorb QUI. However, when synthesis time increases from 15 to 20 h, the QUI/DBT selectivity decreases from 16.0 to 15.2. As mentioned in investigating the effect of synthesis time on adsorption capacity, by prolonging this time, after 15 h the obtained MOFs have a larger particle size, causing long diffusion lengths and hindrance of metal sites of these adsorbents.

The trend of changing selectivity with reagent molar ratio is similar to that with crystallization time. Based on ANOVA, the reagent molar ratio has a 6% contribution percentage in the selectivity model. Since Lewis acid–base and π–M interaction are two major mechanisms for NCC selective adsorption, varying the amount of metal in the MIL-101 structure, which occurred with changes in the reagent molar ratio, can affect QUI/DBT selectivity. Regarding Fig. 3d, the selectivity ratio increased sharply to 0.67 (level 2). It is evident that the possibility of Lewis acid–base and π–M interaction increases with increasing reagent molar ratio and thus with the amount of metal in the unit cell in the synthesis of MOFs. Moreover, at the high reagent molar ratio (> 0.67), QUI/DBT selectivity had an indirect correlation with this ratio. This is explained by the fact that the steric hindrance of metal clusters in MIL-101 increased by raising the metal ratio in MOFs synthesis (Feng and Xia 2018).

3.3 Optimization of NCC adsorption characteristics

As mentioned earlier, the QUI adsorption capacity, QUI/DBT selectivity and arithmetic mean were investigated as three objective functions to optimize effective parameters in MIL-101 synthesis for QUI adsorption from model fuel. Based on the obtained results, it seems that the arithmetic mean is the best response and the objective function for predicting experiment data and optimizing effective parameters in this case.

Based on the model of arithmetic mean of QUI capacity and QUI/DBT selectivity, the optimal conditions were obtained as metal type = Mn, synthesis temperature = 180 °C (which was the maximum studied temperature), synthesis time = 15 h and reagent molar ratio = 0.67. The QUI/DBT selectivity for synthesized adsorbent under optimum conditions was predicted as 23.5 by the model for this selectivity. Due to the optimum condition not presented in the 27 experiments of the orthogonal array, confirming experiments were carried out to judge the predicted results. For the synthesized

adsorbent under optimum conditions, the experimental values of QUI adsorption capacity and QUI/DBT selectivity were obtained as 19.3 mg-N/g-Ads. and 24.6, respectively. According to these results, values of Z^1, which were predicted to be 1.04, were calculated as 1.10. Therefore, it was shown that the experiment and model results were in good agreement with relative errors of just 4.2%. In this case, for simplification, a MIL-101 synthesized under the above optimal conditions was called optimized MIL-101 for ADN (OMA). In the previous studies (Wu et al. 2014; Ahmed and Jhung 2014), the maximum values of QUI adsorption capacity and QUI/DBT selectivity were, respectively, reported 8–11 mg-N/g-Ads and 3.1–12.2, which were much lower than the measured values for OMA.

3.4 The characteristics of optimized adsorbent

Figure 4 presents the XRD patterns of OMA. By evaluating and comparing XRD patterns of this adsorbent, which is MIL-101 (Mn) with similar patterns in the Crystallography Open Database (COD) (Gražulis et al. 2011), it is clear that the OMA was formed from two-phase crystal structures, which are manganese oxide clusters with body-centered tetragonal (tetragonal I) style ($Mn_{12}O_{16}$) and TPA linkers. The X'pert Highscore Plus software was used to refine the XRD data (Domán et al. 2018), resulting in $V = 730 \, Å^3$. This high unit cell volume indicates that the large crystals exist in the OMA skeleton, which can cause high surface area for this adsorbent. Since the OMA is synthesized at high temperature (180 °C), large existing crystals in this MOF skeleton confirm the correct contents and discussions mentioned for describing the effect of temperature on characteristics of synthesized MOFs (Sect. 3.2). Five high-intensity XRD peaks for this adsorbent, which were observed at a 2θ angle of 14.51°, 28.98°, 32.77°, 36.55° and 60.27°, can be assigned to (200), (112), (321), (231) and (244) reflections,
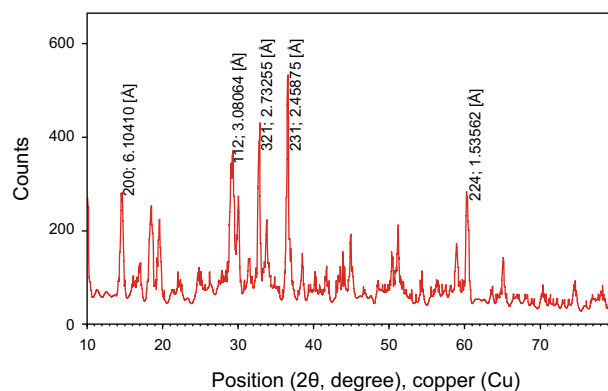

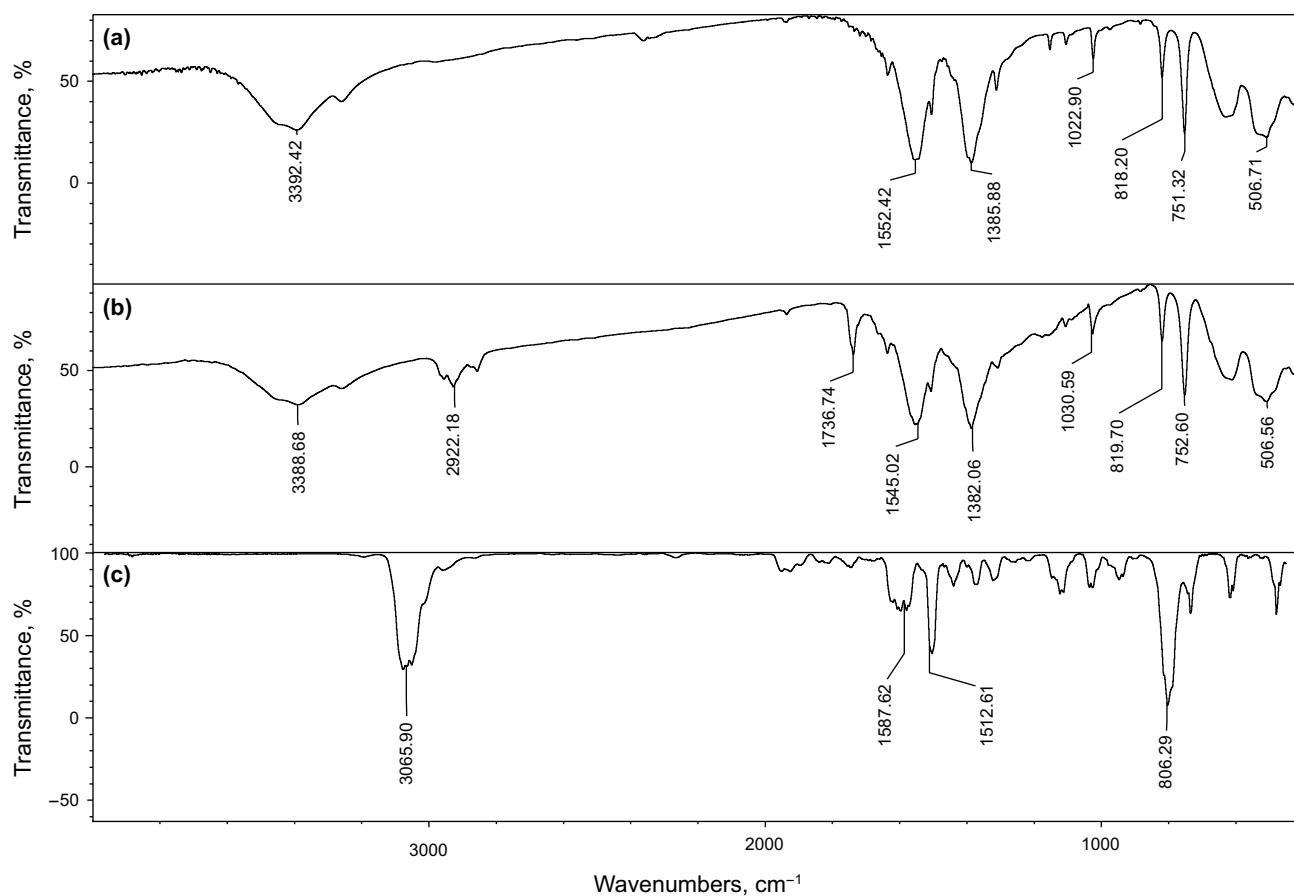**Fig. 4** The X-ray diffraction (XRD) analysis of optimized MIL-101 (OMA)

Fig. 5 FTIR spectra of **a** OMA—before QUI adsorption, **b** OMA—after QUI adsorption and **c** QUI

respectively. 6.1 Å, 3.1 Å, 2.7 Å, 2.5 Å and 1.5 Å are the d spacing of the aforementioned reflections.

The FTIR spectroscopy results of OMA before and after QUI adsorption and QUI are shown in Fig. 5. In Fig. 5a, b, the two big bands at 1385 cm^{-1} and 1552 cm^{-1} are attributed to the metal bond with a carboxylic group (RCOO'M), which appears at 1395–1610 cm^{-1} (Sapchenko et al. 2013; Kuptsov and Zhizhin 1998). Since the carboxylic acid groups (RCOOH) absorption is at 1000–1320 cm^{-1}, the small peak at 1022 cm^{-1} belongs to a few carboxylic groups remaining in the MOFs structure without any changes. These results indicate that the reagents have quite completely reacted and RCOOH groups have reformed to RCOO'M groups (Sapchenko et al. 2013; Kuptsov and Zhizhin 1998). Regarding the database of FTIR spectra (Castro et al. 2003), the peak at 763 cm^{-1} can be attributed to the presence of para-aromatics in this material. Due to the study of Yang et al. (2011), the first peak, which is observable at 506.4 cm^{-1}, indicates the presence of the manganese oxide bond in OMA

By comparing Fig. 5a with b, it is clear that the FTIR pattern of OMA after QUI adsorption has two new peaks at 1737 cm^{-1} and 2922 cm^{-1}. The FTIR spectroscopic results
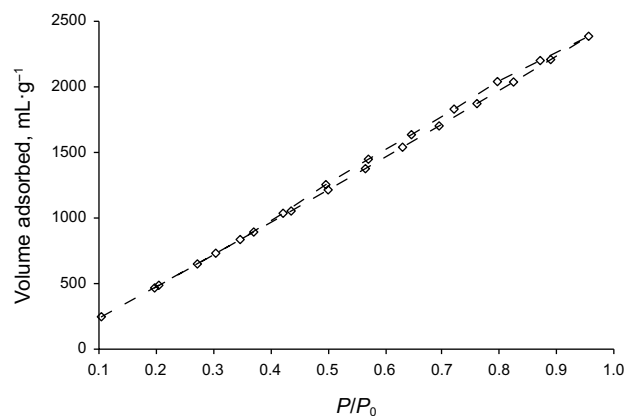

Fig. 6 Adsorption–desorption isotherms of N$_2$ for OMA

of QUI, which are obtained from results of Linstrom and Mallard (2018) and presented in Fig. 5c, were used to investigate the reasons of appearance of two new peaks in FTIR results of OMA after QUI adsorption. Except for the two highlighted peaks which appear at 1700–1800 cm^{-1} and 2900–3100 cm^{-1}, respectively, other peaks of the QUI FTIR

pattern approximately match major peaks of the FTIR pattern of OMA, and the QUI adsorption over the OMA can be determined with these two peaks. Therefore, it can be concluded that the difference between FTIR patterns of OMA before and after QUI adsorption can be attributed to the interaction of QUI with active sites of the adsorbent.

Nitrogen adsorption–desorption isotherms for OMA are presented in Fig. 6, which shows that this isotherm is type II in IUPAC classification. Therefore, it is clear that OMA has a pore structure with a combination of micro- and mesopores. Based on the N_2 isotherms data and BET (Brunauer–Emmett–Teller) and BJH (Barrett–Joyner–Halenda) models (Lowell et al. 2004), BET surface area, total pore volume and average pore diameter were calculated as 4204 m^2 g^{-1}, 3.68 mL g^{-1} and 35 Å, respectively. By comparing these results with characteristics of synthesized MIL-101 in previous studies (Wu et al. 2014; Wang et al. 2013; Ahmed et al. 2013b), it is indicated that the OMA has more suitable surface properties such as higher surface area and pore volume.

3.5 Adsorption isotherms

Figure 7 illustrates the obtained QUI adsorption data and studied isotherm model curves at three different temperatures (20, 30 and 40 °C). In this article, equilibrium data of QUI adsorption on OMA were analyzed by the Langmuir and Freundlich models. Equations (5) and (6) represent the linear forms of the Langmuir and Freundlich models, respectively (Mehrabi et al. 2015; Lyklema 2005).

$$\frac{1}{q_e} = \left(\frac{1}{q_{max}K_L}\right)\frac{1}{C_e} + \frac{1}{q_{max}} \tag{5}$$

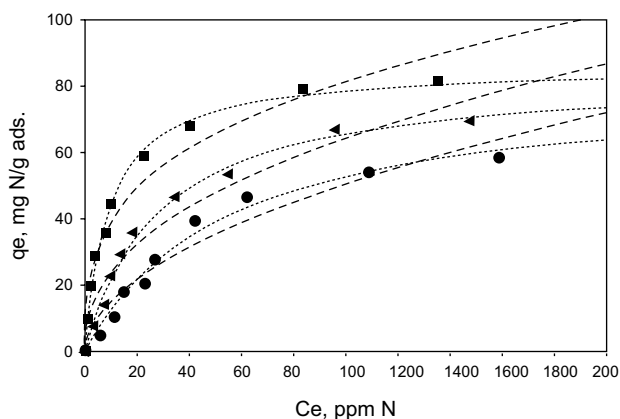$$\log q_e = \frac{1}{n}\log C_e + \log K_f \tag{6}$$

Fig. 7 Adsorption isotherms for QUI over OMA at (filled square) 20 °C, (filled left pointing pointer) 30 °C (V) and (filled circle) 40 °C. Points: experimental data, solid lines: Freundlich's model and dotted lines: Langmuir's model. q_e is the equilibrium adsorption capacity of adsorbents, mg g^{-1}

Here, q_e (mg g^{-1}) is the equilibrium adsorption capacity of adsorbents, q_{max} (mg g^{-1}) is the maximum adsorbed quantity of adsorbate in the Langmuir isotherm and K_L (L mg^{-1}) is a Langmuir constant related to the energy of adsorption. In Eq. 6, K_f ($L^{(1-1/n)}$ $mg^{-1/n}$ g^{-1}) and n are Freundlich constants, related to the adsorption capacity and intensity of adsorbent, respectively.

The calculated parameter values of these isotherm models are reported in Table 4. The results of Fig. 7 and Table 4 (especially R^2 values) prove that the Langmuir model is a more accurate and useful model to estimate the equilibrium data of QUI adsorption on this adsorbent. Since the monolayer assumption is the basic concept of Langmuir theory, it is concluded that a monolayer of QUI is adsorbed on the OMA, which has a homogeneous surface (Lyklema 2005; Mittal and Shah 2005).

The adsorption thermodynamic parameters, including changes in free energy (ΔG), enthalpy (ΔH) and entropy (ΔS), can be calculated by adsorption equilibrium constants (K_L) at different temperatures. These parameters were used to further investigate the adsorption process and determine how QUI adsorbs on OMA. According to Eq. 7, $\Delta H°$ and $\Delta S°$ were determined, respectively, from the slope and intercept of the $\ln(K_L)$ versus $1/T$ plot. Consequently, $\Delta G°$ was calculated by Eq. 8.

$$\ln\left(K_L\right) = \frac{-\Delta H°}{RT} + \frac{\Delta S°}{R} \tag{7}$$

$$\Delta G° = \Delta H° - T\Delta S° \tag{8}$$

where R and T are the universal gas constant (8.314 J mol^{-1} K^{-1}) and temperature (K), respectively. The calculated $\Delta G°$, $\Delta H°$ and $\Delta S°$ for QUI adsorption on OMA are reported in Table 4. The negative values of $\Delta G°$ and $\Delta H°$ of QUI adsorption on this adsorbent indicate that it is a spontaneous exothermic reaction. According to the negative $\Delta S°$, it is evident that the solid/liquid interface entropy

Table 4 Langmuir and Freundlich isotherm and thermodynamic parameters for QUI adsorption over OMA

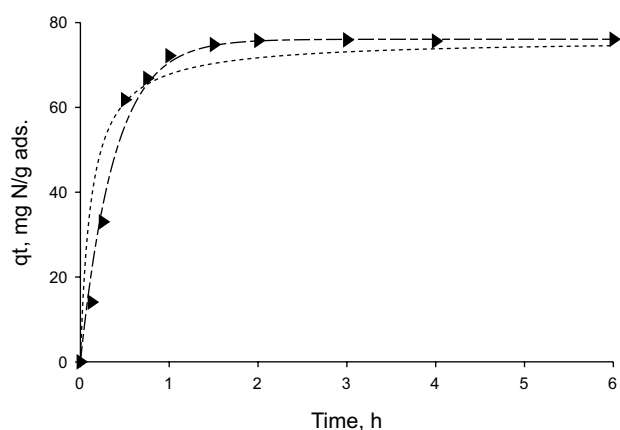| Isotherm	Parameter	Temperature		
		20 °C	30 °C	40 °C
Langmuir	q_{max}, mg g^{-1}	85.82	83.83	81.19
	$K_L \times 10^3$, L mg^{-1}	107.80	35.43	18.39
	R^2	0.9926	0.9928	0.9831
Freundlich	K_f	19.38	8.92	4.63
	N	3.21	2.33	1.93
	R^2	0.9555	0.9541	0.9409
Thermodynamic constant	$\Delta H°$, kJ mol^{-1}		− 67.5873	
	$\Delta S°$, kJ mol^{-1} K^{-1}		− 0.0025	
	$\Delta G°$, kJ mol^{-1}		− 60.0206	

Fig. 8 Effect of contact time on QUI adsorption over OMA (filled right pointing pointer). Points: experimental data, dotted lines: pseudo-first-order model and dot-dash lines: pseudo-second-order model; initial concentrations of QUI = 1000 mg L^{-1} and experimental temperature = 20 °C. q_t is the amount of adsorbed component at time t, mg g^{-1}

decreases by QUI adsorbing on OMA. Since the values of $\Delta G°$ and $\Delta H°$ represent adsorbent tendency, OMA has a high tendency to adsorb QUI. According to the range of calculated $\Delta H°$ and inverse relationship between temperature and q_{max}, it is clear that these MOFs physically adsorb QUI.

3.6 Adsorption kinetics

The QUI adsorption profiles versus time of OMA are presented in Fig. 8. The adsorption type and reaction rate-limited mode such as mass transfer and chemical reaction can be determined from kinetic studies. In this work, two common kinetic models, the pseudo-first-order and pseudo-second-order model, were used to investigate the kinetics of QUI adsorption on OMA. The relationship between the adsorption rate and time in pseudo-first-order and pseudo-second-order models is shown in Eqs. 9 and 10, respectively.

$$\frac{dq}{dt} = k_{p1}(q_e - q_t) \tag{9}$$

$$\frac{dq}{dt} = k_{p2}t(q_e - q_t)^2 \tag{10}$$

where q_e and q_t are the amount of QUI adsorbed at equilibrium and at time t (mg-N/g-Ads), respectively, k_{p1} (s^{-1}) is the reaction rate constant of the pseudo-first-order model and k_{p2} [(g-Ads/mg-N) s^{-1}] is the reaction rate constant of the pseudo-second-order model.

The equations of these kinetic models (Eqs. 9 and 10) were fitted to the experimental data to define rate-limited mode and compare the accuracy of each kinetic model. The values of kinetic parameters were calculated

to be $k_{p1} = 7.29 \times 10^{-4}$ s^{-1} and $k_{p2} = 2.993 \times 10^{-5}$ (g-Ads/mg-N) s^{-1}. The R^2 values for the pseudo-first-order and pseudo-second-order model were calculated as 0.986 and 0.772, respectively. Based on the obtained R^2, it is concluded that the pseudo-first-order model is more accurate and suitable for studying QUI adsorption on OMA. These results demonstrate that QUI adsorption on OMA was controlled by physisorption which verified the results obtained in isotherm studies.

4 Conclusion

In order to improve NCCs removal from fuel, the MIL-101, as a classification of new metal organic frameworks (MOFs), has been synthesized, characterized and used for the ADN process. The Taguchi method and multi-response optimization were applied in synthesizing MIL-101 to find a superior adsorbent for the ADN process. Results of ANOVA showed that the model on the arithmetic mean (Z^1 model) was the most valid one. Based on the Z^1 model, the optimum conditions for MIL-101 synthesis were found to be Mn as metal type, 180 °C (which was the maximum studied temperature) as synthesis temperature, 15 h as synthesis time and 0.67 as reagent molar ratio, where the QUI adsorption capacity and QUI/DBT selectivity were obtained as 19.3 mg-N/g-Ads. and 24.6, respectively. In addition, temperature has the greatest effect of 56%–63% and the reagent molar ratio was not a striking factor in ADN characteristics. The Langmuir isotherm model successfully described the QUI adsorption in equilibrium conditions and indicates that this adsorption takes place at a monolayer coverage on a homogeneous adsorbent surface. Calculated thermodynamic parameters (especially $\Delta H° = 67.59$ kJ mol^{-1}) and kinetic studies results (experimental data following the pseudo-first-order model) demonstrate that QUI adsorption on MIL-101 might involve physisorption.

References

Aghaei E, Haghighi M. Effect of crystallization time on properties and catalytic performance of nanostructured SAPO-34 molecular sieve synthesized at high temperatures for conversion of methanol to light olefins. Powder Technol. 2015;269:358–70. https://doi.org/10.1016/j.powtec.2014.09.036.

Ahmed I, Hasan Z, Khan NA, Jhung SH. Adsorptive denitrogenation of model fuels with porous metal-organic frameworks (MOFs): effect of acidity and basicity of MOFs. Appl Catal B Environ. 2013a;129:123–9. https://doi.org/10.1016/j.apcatb.2012.09.020.

Ahmed I, Jhung SH. Adsorptive denitrogenation of model fuel with CuCl-loaded metal-organic frameworks (MOFs). Chem Eng J. 2014;251:35–42. https://doi.org/10.1016/j.cej.2014.04.044.

Ahmed I, Jhung SH. Adsorptive desulfurization and denitrogenation using metal-organic frameworks. J Hazard Mater. 2016;301:259–76. https://doi.org/10.1016/j.jhazmat.2015.08.045.

Ahmed I, Khan NA, Jhung SH. Graphite oxide/metal-organic framework (MIL-101): remarkable performance in the adsorptive denitrogenation of model fuels. Inorg Chem. 2013b;52(24):14155–61. https://doi.org/10.1021/ic402012d.

Antony J. Multi-response optimization in industrial experiments using Taguchi's quality loss function and principal component analysis. Qual Reliab Eng Int. 2000;16(1):3–8. https://doi.org/10.1002/(SICI)1099-1638(200001/02)16:1%3c3:AID-QRE276%3e3.0.CO;2-W.

Bag PP, Wang X-S, Cao R. Microwave-assisted large scale synthesis of lanthanide metal-organic frameworks (Ln-MOFs), having a preferred conformation and photoluminescence properties. Dalton Trans. 2015;44(26):11954–62. https://doi.org/10.1039/C5DT01598G.

Castro K, Pérez M, Rodríguez-Laso MD, Madariaga JM. Peer reviewed: FTIR spectra database of inorganic art materials. Washington: ACS Publications; 2003. https://doi.org/10.1021/ac031320e.

Domán A, Nagy B, Nichele LP, Srankó D, Madarász J, László K. Pressure resistance of copper benzene-1,3,5-tricarboxylate–carbon aerogel composites. Appl Surf Sci. 2018;434:1300–10. https://doi.org/10.1016/j.apsusc.2017.11.251.

Feng D, Xia Y. Comparisons of glyphosate adsorption properties of different functional Cr-based metal-organic frameworks. J Sep Sci. 2018;41(3):732–9. https://doi.org/10.1002/jssc.201700886.

Gražulis S, Daškevič A, Merkys A, Chateigner D, Lutterotti L, Quiros M, et al. Crystallography Open Database (COD): an open-access collection of crystal structures and platform for world-wide collaboration. Nucleic Acids Res. 2011;40(D1):D420–7. https://doi.org/10.1093/nar/gkr900.

Guria C, Goli KK, Pathak AK. Multi-objective optimization of oil well drilling using elitist non-dominated sorting genetic algorithm. Pet Sci. 2014;11(1):97–110. https://doi.org/10.1007/s12182-014-0321-x.

Heidari H, Razmi H. Multi-response optimization of magnetic solid phase extraction based on carbon coated Fe_3O_4 nanoparticles using desirability function approach for the determination of the organophosphorus pesticides in aquatic samples by HPLC–UV. Talanta. 2012;99:13–21. https://doi.org/10.1016/j.talanta.2012.04.023.

Hu M-L, Safarifard V, Doustkhah E, Rostamnia S, Morsali A, Nouruzi N, et al. Taking organic reactions over metal-organic frameworks as heterogeneous catalysis. Micropor Mesopor Mater. 2018;256:111–27. https://doi.org/10.1016/j.micromeso.2017.07.057.

Khan NA, Uddin N, Choi CH, Jhung SH. Adsorptive denitrogenation of model fuel with CuCl-loaded adsorbents: contribution of Π-complexation and direct interaction between adsorbates and cuprous ions. J Phys Chem C. 2017;121(21):11601–8. https://doi.org/10.1021/acs.jpcc.7b03369.

Kuptsov A, Zhizhin GN. Handbook of Fourier transform Raman and infrared spectra of polymers. Amsterdam: Elsevier; 1998.

Lyklema J. Langmuir monolayers. In: Lyklema J, editor. Fundamentals of interface and colloid science: soft colloids, vol. V. Amsterdam: Elsevier Academic Press; 2005. p. 3.1–3.247. https://doi.org/10.1016/s1874-5679(00)80006-9.

Li J-R, Ma Y, McCarthy MC, Sculley J, Yu J, Jeong H-K, et al. Carbon dioxide capture-related gas adsorption and separation in metal-organic frameworks. Coord Chem Rev. 2011;255(15–16):1791–823. https://doi.org/10.1016/j.ccr.2011.02.012.

Li Q, Zhang Y, Cao Z, Gao W, Cui L. Crystallization behavior of zeolite beta from acid-leached metakaolin. Pet Sci. 2010a;7(4):541–6. https://doi.org/10.1007/s12182-010-0106-9.

Li Q, Zhang Y, Cao Z, Gao W, Cui L. Influence of synthesis parameters on the crystallinity and Si/Al ratio of NaY zeolite synthesized from kaolin. Pet Sci. 2010b;7(3):403–9. https://doi.org/10.1007/s12182-010-0085-x.

Linstrom PJ, Mallard WG. NIST Standard Reference Database Number 69. NIST Chemistry WebBook. 2018. https://doi.org/10.18434/t4d303.

Loloie Z, Mozaffarian M, Soleimani M, Asassian N. Carbonization and CO_2 activation of scrap tires: optimization of specific surface area by the Taguchi method. Korean J Chem Eng. 2017;34(2):366–75. https://doi.org/10.1007/s11814-016-0266-4.

Lowell S, Shields J, Thomas M, Thommes M. Characterization of porous materials and powders: surface area, pore size and density. Dordrecht: Springer; 2004. https://doi.org/10.1007/978-1-4020-2303-3.

Mehrabi N, Soleimani M, Yeganeh MM, Sharififard H. Parameter optimization for nitrate removal from water using activated carbon and composite of activated carbon and Fe_2O_3 nanoparticles. RSC Adv. 2015;5(64):51470–82. https://doi.org/10.1039/C5RA03920G.

Mittal KL, Shah DO. Adsorption and aggregation of surfactants in solution. New York: Taylor & Francis; 2005.

Moattari RM, Rahimi S, Rajabi L, Derakhshan AA, Keyhani M. Statistical investigation of lead removal with various functionalized carboxylate ferroxane nanoparticles. J Hazard Mater. 2015;283:276–91. https://doi.org/10.1016/j.jhazmat.2014.08.025.

Montgomery DC. Design and analysis of experiments. Hoboken: Wiley; 2017.

Rahimi S, Moattari RM, Rajabi L, Derakhshan AA. Optimization of lead removal from aqueous solution using goethite/chitosan nanocomposite by response surface methodology. Colloid Surf A. 2015a;484:216–25. https://doi.org/10.1016/j.colsurfa.2015.07.063.

Rahimi S, Moattari RM, Rajabi L, Derakhshan AA, Keyhani M. Iron oxide/hydroxide (α, γ-FeOOH) nanoparticles as high potential adsorbents for lead removal from polluted aquatic media. J Ind Eng Chem. 2015b;23:33–43. https://doi.org/10.1016/j.jiec.2014.07.039.

Safarzadeh MA, Motahhari SM. Co-optimization of carbon dioxide storage and enhanced oil recovery in oil reservoirs using a multi-objective genetic algorithm (NSGA-II). Pet Sci. 2014;11(3):460–8. https://doi.org/10.1007/s12182-014-0362-1.

Sapchenko SA, Samsonenko DG, Fedin VP. Synthesis, structure and luminescent properties of metal-organic frameworks constructed from unique Zn- and Cd-containing secondary building blocks. Polyhedron. 2013;55:179–83. https://doi.org/10.1016/j.poly.2013.03.031.

Seetharaj R, Vandana P, Arya P, Mathew S. Dependence of solvents, pH, molar ratio and temperature in tuning metal organic framework architecture. Arab J Chem. 2016. https://doi.org/10.1016/j.arabjc.2016.01.003.

Sentorun-Shalaby C, Ma X, Song C. Preparation of high-performance adsorbent from coal for adsorptive denitrogenation of liquid hydrocarbon streams. Energy Fuels. 2013;27(3):1337–46. https://doi.org/10.1021/ef400008x.

Songolzadeh M, Soleimani M, Takht Ravanchi M. Evaluation of metal type in MIL-100 structure to synthesize a selective adsorbent for the basic N-compounds removal from liquid fuels. Micropor

Mesopor Mater. 2019;274:54–60. https://doi.org/10.1016/j.micromeso.2018.07.032.

Stock N, Biswas S. Synthesis of metal-organic frameworks (MOFs): routes to various MOF topologies, morphologies, and composites. Chem Rev. 2011;112(2):933–69. https://doi.org/10.1021/cr200304e.

Taheri A, Babakhani EG, Towfighi J. Study of synthesis parameters of MIL-53 (Al) using experimental design methodology for CO_2/CH_4 separation. Adsorpt Sci Technol. 2018;36(1–2):247–69. https://doi.org/10.1177/0263617416688690.

Wang Z, Sun Z, Kong L, Li G. Adsorptive removal of nitrogen-containing compounds from fuel by metal-organic frameworks. J Energy Chem. 2013;22(6):869–75. https://doi.org/10.1016/S2095-4956(14)60266-7.

Wee LH, Lohe MR, Janssens N, Kaskel S, Martens JA. Fine tuning of the metal-organic framework Cu3(BTC)2 HKUST-1 crystal size in the 100 nm to 5 micron range. J Mater Chem. 2012;22(27):13742–6. https://doi.org/10.1039/C2JM31536J.

Wu Y, Xiao J, Wu L, Chen M, Xi H, Li Z, et al. Adsorptive denitrogenation of fuel over metal organic frameworks: effect of N-types and adsorption mechanisms. J Phys Chem C. 2014;118(39):22533–43. https://doi.org/10.1021/jp5045817.

Yang S, Yang H, Ma H, Guo S, Cao F, Gong J, et al. Manganese oxide nanocomposite fabricated by a simple solid-state reaction and its ultraviolet photoresponse property. Chem Commun. 2011;47(9):2619–21. https://doi.org/10.1039/C0CC04783J.

Zhang B, Hao S, Xiao D, Wu J, Huang Y. Templated formation of porous Mn_2O_3 octahedra from Mn–MIL-100 for lithium-ion battery anode materials. Mater Des. 2016;98:319–23. https://doi.org/10.1016/j.matdes.2016.03.041.

Zhang CY, Wang MY, Li QT, Qian BH, Yang XJ, Xu XY. Hydrothermal synthesis, crystal structure, and luminescent properties of two zinc(II) and cadmium(II) 3D metal-organic frameworks. Z Anorg Allg Chem. 2013;639(5):826–31. https://doi.org/10.1002/zaac.201200473.